Lymphatic Biodistribution of Polylactide Nanoparticles

Eric J. Chaney, Li Tang, Rong Tong, Jianjun Cheng, and Stephen A. Boppart

Abstract

Tumor metastases occur through both the cardiovascular and lymphatic circulations. However, the majority of nanoparticle biodistribution studies have been focused on the cardiovascular circulation. In this study, we report the formulation of Cy5-labeled polylactide (Cy5-PLA) nanoparticles with controlled size and surface features and the subsequent evaluation of their lymphatic biodistribution. Cy5-PLA nanoparticles were formulated through Cy5/(BDI)ZnN(TMS)$_2$-mediated [(BDI) = 2-((2,6-diisopropylphenyl) amido)-4-((2,6-diisopropylphenyl)-imino)-2-pentene] ring-opening polymerization of lactide followed by nanoprecipitation. Their lymphatic biodistribution was evaluated by using whole-body fluorescence imaging of nude mice and ex vivo fluorescence imaging of the resected organs. This technique has the potential for providing optical contrast and drug delivery through the lymphatic circulation for the treatment of metastatic cancer.

METASTATIC CANCER disseminates through not only the cardiovascular circulation but also the lymphatic circulation. Compared to the cardiovascular circulation, the lymphatic circulation is more optimally suited for the entry, transport, and seeded growth of metastatic cells.[1] Even the smallest lymphatic vessels have larger diameters than blood capillaries and provide lower flow velocity. Tumor cells in the lymphatic vessels typically experience less serum toxicity and lower destructive mechanical deformation because of reduced shear stresses, which favor metastatic tumor formation.[2,3] Therefore, metastases via the lymphatics are potentially more efficient than via the cardiovascular system.[4] A recent study indicates that the presence of tumor cells in lymph nodes has strong correlation with primary tumor metastasis and tumor recurrence.[5] Although tumor metastasis is relatively slow and only a small portion of the metastatic cells from the primary tumor form secondary tumors,[6–10] the 5-year patient survival rates fall precipitously once tumor metastases occur. Therefore, developing effective systems that allow for treatment of metastatic cancer in the lymphatic system is of significant clinical importance and may substantially improve the survival rates of metastatic cancer.

Nanoparticle (NP)-based drug delivery technologies can potentially provide effective and sustained treatment for metastatic cancer. In the past decade, a number of NP delivery systems have been developed for treating cancer, and their in vivo systemic biodistribution has been extensively studied. However, the majority of NP biodistribution studies have focused on the cardiovascular circulation system.[11–13] Although some studies are using quantum dots as diagnostic modalities,[14–16] few studies have been performed to assess the biodistribution of drug delivery NPs through the lymphatic circulatory system, providing limited information and guidance for the treatment of metastatic cancer in the lymphatic system.

We fabricated and studied the lymphatic biodistribution of polylactide (PLA) nanoparticles, a class of polymeric nanoparticles (PNPs) drug delivery systems that have been previously investigated.[17,18] The Cy5-PLA conjugates were prepared via a unique Cy5-initiated ring-opening polymerization of lactide (LA).[19–21] The resulting Cy5-PLA conjugates can facilitate the preparation of biodegradable PNPs for fluorescence imaging studies. The Cy5 molecules are covalently linked to PLA and therefore have reduced release kinetics compared to PNPs prepared via coprecipitation of PLA and Cy5. In PNPs prepared via coprecipitation, the Cy5 molecules are embedded in the PLA matrices and typically show large "burst" release kinetics in solution, prohibiting the

From the Beckman Institute for Advanced Science and Technology; Departments of Materials Science and Engineering, Chemistry, Electrical and Computer Engineering, Bioengineering, and Medicine; and Micro and Nanotechnology Laboratory, University of Illinois at Urbana-Champaign, Urbana, IL.

Address reprint requests to: Stephen A. Boppart, MD, PhD, University of Illinois at Urbana-Champaign, 405 N. Mathews Avenue, Urbana, IL 61801; e-mail: boppart@illinois.edu.

DECKER℞

accurate assessment of NP biodistribution in vivo. We selected Cy5 to be incorporated into the PNPs because Cy5 has an emission band (λ_{em} = 673 nm) in the red wavelength region, resulting in Cy5-PLA PNPs that emit fluorescence signals that are poorly absorbed by tissue. We report the feasibility of this unprecedented strategy for preparing red-fluorescent PLA-Cy5 conjugates and PNPs with sub–100 nm sizes that can be used as a model drug delivery system to study the lymphatic biodistribution of PNPs when coupled with whole-body optical imaging techniques.

Materials and Methods

General

For this study, LA was purchased from TCI America (Portland, OR), recrystallized three times in toluene, and stored at −30°C in a glovebox prior to use. The BDI ligands [(BDI) = 2-((2,6-diisopropylphenyl)amido)-4-((2,6-diiso-propylphenyl)-imino)-2-pentene] and the corresponding metal catalysts ((BDI)ZnN(TMS)$_2$) were prepared by following published procedures[22] and stored at −30°C in a glovebox prior to use. All anhydrous solvents were purified by passing them through dry alumina columns and kept anhydrous using molecular sieves. The Cy5 was synthesized according to a published procedure.[23] All other chemicals were purchased from Sigma-Aldrich (St Louis, MO) and used as received, unless otherwise specified.

The molecular weight (MWs) of the PLA and Cy5-PLA were determined on a gel permeation chromatograph (GPC; also called size-exclusion chromatography) equipped with an isocratic pump (Model 1100, Agilent Technology, Santa Clara, CA), a DAWN HELEOS 18-angle laser light scattering detector (Wyatt Technology, Santa Barbara, CA), and an Optilab rEX refractive index detector (Wyatt Technology). The wavelength of the HELEOS detector was set at 658 nm. The size exclusion columns used for the separation of PLA and Cy5-PLA conjugates were series-connected on the GPC (Phenogel columns 100, 500, 10^3, and 10^4 Å, 5 µm, 300 × 7.8 mm, Phenomenex, Torrance, CA). Tetrahydrofuran (THF) (high-performance liquid chromatography [HPLC] grade) was used as the mobile phase of GPC. HPLC analyses were performed on a System Gold system (Beckman Coulter, Fullerton, CA) equipped with a 126P solvent module, a System Gold 128 ultraviolet (UV) detector, and an analytic pentafluorophenyl column (Curosil-PFP, 250 × 4.6 mm, 5 µm, Phenomenex) or an analytic C18 column (Luna C18, 250 × 4.6 mm, 5 µm, Phenomenex). The UV wavelength

for detecting Cy5 was set at 550 nm. The nuclear magnetic resonance (NMR) experiments were conducted on a Varian U500, a VXR500, or a UI500NB (500 MHz) NMR spectrometer. The size and particle dispersity of the PLA-Cy5 NPs were measured on a ZetaPlus Dynamic Light Scattering (DLS) detector (15 mW laser, incident beam = 676 nm; Brookhaven Instruments, Holtsville, NY). The transmission electron microscopy (TEM) analysis was performed on a JEOL 2100 Cryo-TEM system.

Preparation of Cy5-PLA Conjugate

In a glovebox, Cy5 (5.1 mg, 0.01 mmol) was dissolved in anhydrous THF (1 mL). (BDI)ZnN(TMS)$_2$ (7.0 mg, 0.011 mmol) in THF (100 µL) was added to the Cy5 solution. The mixture was stirred for 15 to 20 minutes at room temperature. LA (144 mg, 1.0 mmol) in THF (2 mL) was added dropwise to the vigorously stirred mixture of Cy5 and (BDI)ZnN(TMS)$_2$. The polymerization was monitored by following the lactone band at 1,772 cm^{-1} using Fourier transform infrared spectroscopy (FTIR) or by checking the methine (−CH−) peak of LA using ^{1}H NMR. After the polymerization was complete, and to determine the incorporation efficiency of Cy5 to the Cy5-PLA conjugate, an aliquot of the polymerization solution was measured by HPLC to quantify the unreacted Cy5. The resulting Cy5-PLA was precipitated with methanol/acetic acid (v/v = 100/1, 10 mL) to remove BDI ligand and dried under vacuum. Complete removal of BDI was confirmed by NMR, HPLC, and thin-layer chromatography (TLC) . After the organic solvent was evaporated, the residue was dissolved in HPLC grade THF (10 mg/mL) and analyzed by GPC with THF (HPLC grade) being used as the mobile phase. The flow rate was set as 1 mL/min.

Cy5-PLA-conjugated NPs were readily prepared through the nanoprecipitation of Cy5-PLA conjugates in the presence of PLA-monomethoxy poly(ethylene glycol) (PLA-mPEG) (Figure 1).[17,18] Briefly, Cy5-PLA conjugate in *N,N*-dimethylformamide (DMF) (100 µL, 10 mg/mL) and PLA-mPEG in *N,N*-dimethylformamide (DMF) (100 µL, 10 mg/mL) were added dropwise into a nonsolvent of 20× nanopure water (4 mL). The resulting NP suspension was purified by ultrafiltration (15 minutes, 3,000 rpm, Ultracel membrane with 10,000 NMWL, Millipore, Billerica, MA) and then characterized by DLS and TEM.

Animal Studies

Animal care and handling was performed under a protocol approved by the Institutional Animal Care and Use

Committee at the University of Illinois at Urbana-Champaign. Athymic nude mice *nu/nu* (Harlan, Indianapolis, IN), chosen for their small size and thin hairless skin that allow for both in vivo and ex vivo optical imaging, were anesthetized by intraperitoneal injection with a combination of ketamine (100 mg/kg) and xylazine (10 mg/kg). To deliver the Cy5-PLA PNPs into the lymphatic circulation, PNPs (20–25 μL, 10 mg/mL in saline) were injected into the interstitial space of the left footpad of two mice. An equal volume of sterile saline was injected into the right footpads. An additional mouse was injected with sterile saline into the left footpad to be used as a control. The footpads were chosen because they provide direct access to the lymphatic system[24] of rodents and drain directly to the popliteal lymph nodes. Each mouse was imaged in vivo prior to and immediately after the PNP administration. In vivo whole-body and isolated organ fluorescence imaging were performed on a Maestro Imaging System (CRi, Inc.; Woburn, MA, excitation 575–605 nm, emission 655 nm longpass) and a predetermined exposure time. The animals were allowed to recover and then were reanesthetized and reimaged after 24 hours. After the second imaging session, the animals were sacrificed. The right and left popliteal lymph nodes, spleen, liver, lung, brain, heart, and kidneys were harvested and imaged ex vivo, using comparable organs from a noninjected animal as negative controls.

To compare the biodistribution of our NPs between the cardiovascular and lymphatic systems, an additional animal was injected with an equal concentration and volume of PNPs into the cardiovascular system via a tail vein. The animal and organs were imaged as described above.

Statistical Analysis

Using a predetermined area of interest (AOI) in each image, the average fluorescence intensity was measured and quantified using commercial software (*Maestro*, CRi, Inc.) to determine the average fluorescence within a defined region. Because the fluorescence signal observed in each individual organ was not homogeneously distributed throughout the organ, six random AOI regions across each organ were selected, and the total fluorescence per area was measured and averaged across the six areas to determine the average fluorescence intensity. The calculated standard deviation was determined between the six AOIs, not between the animals. The paired Student *t*-test was applied to the quantified fluorescence from each organ and the

control, as well as between the two different injection methods.

Results and Discussion

Interest is growing in developing noninvasive, whole-body animal fluorescent imaging techniques to assess the biodistribution of drug delivery systems or diagnostic agents. To ensure effective measurement of fluorescent signal in vivo, it is crucial to use red or near-infrared dyes. Quantum dots, a class of inorganic nanocrystals with excellent fluorescent intensity and photostability, can be readily prepared to have a far-red emission band. However, there is a general consensus that quantum dots cannot be used in humans because of their severe toxicity.[25,26] Also, various in vivo imaging modalities, such as magnetic resonance imaging[27–29] and photoacoustics,[30,31] using different kinds of NPs, are currently being explored to map lymphatic vessels and lymph nodes that potentially could be carrying metastatic cancer cells. Therefore, NPs and small molecule organic dyes are promising probes that can be coupled with imaging systems for clinical applications.

PNPs are important carriers for the delivery of chemotherapeutics or imaging materials because they can provide prolonged systemic circulation and improved tumor accumulation compared to unformulated drugs.[32–37] To evaluate the lymphatic biodistribution of PNPs, it is particularly important to formulate PNPs with stably incorporated fluorescent ligands and controlled formulation parameters (eg, size, surface properties). A number of techniques have been developed for the formulation of PNPs. One of the most widely used techniques is called nanoprecipitation. Nanoprecipitation allows for the formulation of PNPs via the coprecipitation of a hydrophobic polymer and a hydrophobic drug (dye) into aqueous solution. The resulting PNPs hold particular promise because of their easy formulation and potential control of drug release through the degradation of polymers. However, current PNPs prepared via nanoprecipitation techniques show low drug (dye) loadings,[38,39] uncontrollable encapsulation efficiency,[39,40] and significant drug (dye) burst release profiles,[38] all of which significantly limit the utility of nanoprecipitation as a means to formulate PNPs suitable for in vivo biodistribution studies and eventual clinical utility.

We aimed to incorporate Cy5, a red cyanine dye with an excitation wavelength of 656 nm and an emission wavelength of 673 nm (Figure 2A), to PLA to create a class of fluorescent NPs that can be used for in vivo imaging. However, given that Cy5 is water soluble, it is impossible
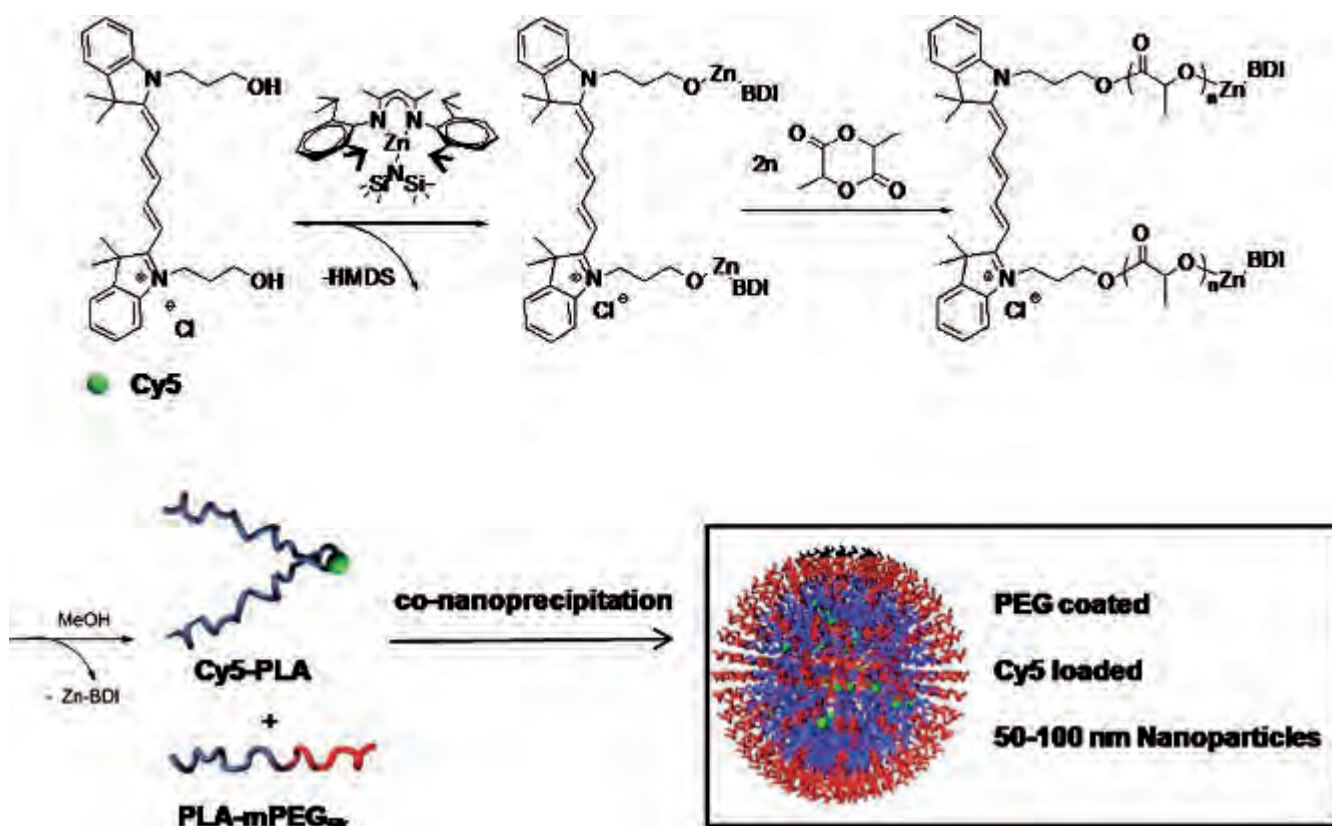
Figure 1. Preparation of poly(ethylene glycol)ated (PEGylated) Cy5-PLA nanoparticles for lymphatic system tracking by means of Cy5-initiated LA polymerization in the presence of (BDI)ZnN(TMS)$_2$, followed by co-nanoprecipitation with polylactide-*b*-methoxylated PEG (PLA-mPEG$_{5K}$).
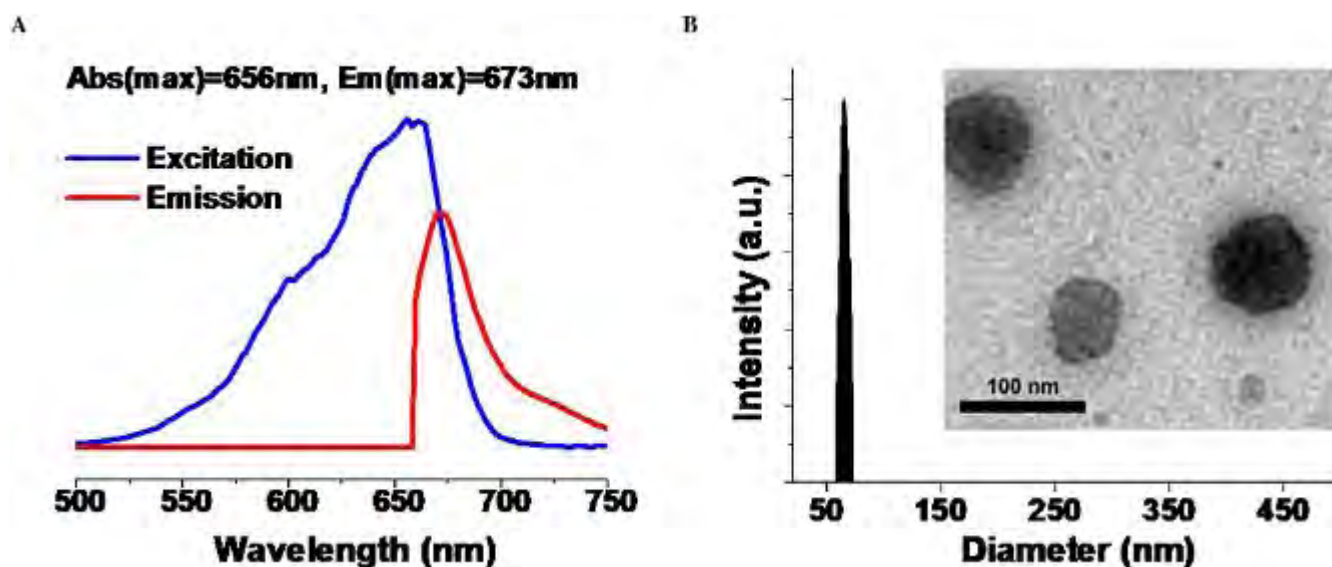

Figure 2. Polymer and nanoparticle properties. *A*, Excitation and emission of the Cy5-PLA polymer, with the maximum absorption at 656 nm and the maximum emission at 673 nm. *B*, Plot of a single distribution of Cy5-PLA/PLA-mPEG$_{5k}$ nanoparticles analyzed by dynamic light scattering. Transmission electron microscopy (*inset*) demonstrates uniform particle size.

to formulate Cy5-PLA PNPs via the nanoprecipitation method with Cy5 stably incorporated to PNPs. Here we test the use of Cy5 as an initiator for LA polymerization to finish Cy5-PLA synthesis during the process of a controlled polymerization to allow Cy5 conjugated to the termini in PLA chains. We then nanoprecipitated Cy5-PLA conjugates to make PNPs with Cy5 stably incorporated.

To ensure rapid and complete polymerization of LA at room temperature using Cy5 as the initiator, we used $(BDI)ZnN(TMS)_2$, an active catalyst developed for the polymerization of LA (see Figure 1).[22] We have previously reported initiation of paclitaxel followed by controlled polymerization of LA when the polymerization was mediated by $(BDI)ZnN(TMS)_2$.[21] After paclitaxel was mixed with 1 equiv. $(BDI)ZnN(TMS)_2$, the (BDI)Zn-paclitaxel alkoxide formed in situ via the $2'$-OH, and the polymerization of LA was completed within hours at room temperature with nearly complete incorporation of paclitaxel into the resulting PLA. Because Cy5 has two hydroxyl groups, we anticipated that Cy5-PLA conjugates could be similarly prepared by using this method. Cy5 is thus stably incorporated with PLA, as releasing Cy5 from Cy5-PLA conjugates requires the cleavage of two esters bonds (see Figure 1).

We prepared Cy5-PLA via Cy5/$(BDI)ZnN(TMS)_2$-mediated LA polymerization at an LA to Cy5 ratio of 100. The obtained M_n of Cy5-PLA was 1.27×10^4 g/mol, which was in good agreement with the expected MW (1.52×10^4 g/mol). The Cy5-PLA also had a very narrow molecular weight distribution (MWD; $M_w/M_n = 1.03$), which is consistent with what we reported previously for $(BDI)ZnN(TMS)_2$-mediated initiation with the paclitaxel and controlled LA polymerization.[21] Cy5-PLA conjugates prepared at an LA to Cy5 ratio of 200 and 300 were also synthesized using the same method with expected M_n's and very narrow MWDs (data not shown). It has been shown that the release of drug (dye) can be further reduced by incorporating drug (dye) molecules into PLA with higher MWs.[19,21] Syntheses of Cy5-PLA conjugates are straightforward. Gram-scale Cy5-PLA conjugates with well-controlled composition and well-controlled MWs can be easily prepared using this drug-initiated polymerization method and used for the preparation of Cy5-PLA PNPs.

Nanoprecipitation has been extensively used for the preparation of NPs with therapeutic agents embedded in the hydrophobic polymeric matrices.[17,18,41] The nanoprecipitation method allows for rapid access to NPs in large quantity. Typically, a mixture of hydrophobic polymer and drug is dissolved in water-miscible organic solvent (eg, DMF or acetone) and then added dropwise to a vigorously stirred water

solution ($V_{water}/V_{solvent} = 10$ to 40). The instantaneous diffusion of the organic solvent into water results in formation of polymer/drug NPs. The nanoprecipitation of Cy5-PLA resulted in Cy5-PLA PNPs 64.5 ± 0.9 nm in size with monomodal particle size distributions and low polydispersities (Figure 2B). The narrow, monomodal particle size distributions for PNPs derived from the Cy5-PLA conjugates have also been confirmed by TEM and are in sharp contrast to the multimodal particle size distribution typically observed with the NPs prepared by the coprecipitation of a mixture of drug (dye) molecule and hydrophobic polymer (eg, PLA or PLGA [poly(lactide-co-glycolide)]).[18] The multimodal distribution of NPs is due in part to the aggregation of the nonencapsulated drug molecules.[18] The monomodal particle size distribution pattern observed and the very low polydispersities with the Cy5-PLA PNP are likely related to the unimolecular structures of the Cy5-PLA conjugates.

The lymphatic circulation is critically involved in the metastatic spread of cancer cells, and tumor metastasis to regional lymph nodes is an established clinical criterion for determining the stage of the disease and directing therapeutic options. Once tumor cells enter the lymphatic circulation, lymph nodes can even actively facilitate the process by which tumor cells spread to other parts of the body.[42,43] Lymphatic biodistribution for drug delivery could eventually become an independent or an adjunct therapy for targeting metastatic cancer or primary hematologic malignancies, such as lymphomas and leukemias. Therefore, it is of great clinical significance to understand the biodistribution of these PNPs and determine if they can efficiently be transported via the lymphatic circulation.

To test this, once the PNPs were conjugated, they were injected into a nude mouse model for evaluation of their lymphatic and cardiovascular circulation biodistribution. Figure 3 shows representative images from in vivo whole-body imaging of a footpad-injected mouse, as well as the various excised tissues and their controls. At 0 hours, immediately after injection, fluorescence was seen only at the site of injection. After 24 hours, the fluorescent signal at the injection site was slightly less, and weak signal could be seen within the abdominal region and elsewhere. The individual ex vivo organ images in Figure 3 demonstrate that the PNPs had distributed from the site of injection in the left footpad into the lymphatic circulation, through the popliteal lymph node, and even to the right side of the animal, including the right popliteal lymph node.

Interestingly, a visually strong fluorescence was observed from the lungs of the injected animal. This could be due to the size or the charge of the PNPs, which likely limit their ability to pass through the blood capillaries of

the lungs after the PNPs have left the lymphatic circulation and entered the cardiovascular circulation via the thoracic duct. Some of the PNPs did pass out of the lungs, as observed in the right popliteal lymph nodes, which could have occurred only if the PNPs passed from the lymphatic circulation, into the cardiovascular circulation, and then into the right-sided lymph nodes. Expectedly, the fluorescence from the right popliteal lymph node is less than the signal from the left popliteal lymph node.

To validate the above results and to quantify and compare the biodistribution of the PNPs, a second experiment was conducted in which two animals were injected with Cy5-PLA PNPs either by tail vein or tissue injection into the lymphatics (via the footpad). In one animal, the PNPs were delivered into the lymphatic system by injection into the footpad, as before. The second animal was injected with an equal concentration and volume of PNPs into the cardiovascular circulation via a tail vein. The imaging procedure of the animals and tissues was conducted as previously described. With the exception of the liver, the fluorescence from the organs of the footpad-injected animals was greater and statistically significant ($p < .05$) compared to the control tissues. This demonstrates that the Cy5-conjugated PNPs had distributed throughout the lymphatic and cardiovascular circulation within 24 hours. The biodistribution of the tail vein–injected PNPs was also statistically significant ($p < .05$) in most of the organs compared to the control organs, with the exception being the left popliteal lymph node.

Surprisingly, we saw large signal from the right popliteal lymph node of the tail vein–injected animal. This could be the result of better circulation and distribution of a higher concentration of PNPs to that area compared to the PNP biodistribution through the lymphatic system, where the PNPs originated from the left-side lymphatics and required passage through the lung capillary bed, before being distributed systemically via the cardiovascular circulation. Alternatively, these observed results could be due to physiologic differences in the circulation or flow or the normal or reactive state of the different lymph nodes in this particular animal. However, it is not surprising that the biodistribution to the left popliteal lymph node is greater for the footpad-injected animal than for the tail vein–injected animal, also being statistically significant ($p < .05$). Most importantly, the distribution of PNPs to the popliteal lymph nodes (both right and left) is statistically significant between delivery routes through the lymphatic versus the cardiovascular circulations, suggesting that the lymphatic circulation may provide for more efficient delivery than the cardiovascular

circulation when attempting to target lymphatic metastases. Based on these results from this feasibility study, future experiments are planned with larger animal numbers to determine variations in pharmacokinetics between animals.

As seen in Figure 4, there is a greater Cy5 fluorescence signal from the kidneys of the tail vein–injected animal compared to the kidneys from both the footpad-injected animal and the control. Our data suggest that a greater number of PNPs introduced into the cardiovascular circulatory system are more rapidly excreted by the kidneys compared to those introduced though the lymphatic circulation. The significance and potential benefit of reduced clearing for lymphatic drug delivery remain to be determined. Further quantitative pharmacokinetic and clearance studies are needed to confirm these findings.

One possible concern is the hydrolysis of the ester bond–linked Cy5 from the PNPs. Although the release kinetics of Cy5 has been reduced dramatically by incorporating Cy5 with two PLA segments via ester bonds, the release of Cy5 would still result in some of the observed fluorescence being emitted from free Cy5 dye. The amount of fluorescence observed in the brain from an animal injected with Cy5-PNPs in the footpad was quantified and compared to the brain of an animal injected in the footpad with free Cy5 dye (Figure 5). Both injected volumes were allowed to circulate for 24 hours through the lymphatic system. Our results from the brain specimens suggest that after 24 hours of circulation, approximately half of the Cy5-PLA PNPs remain intact or accumulate at sites that do not allow them to approach the blood-brain barrier. It has been demonstrated that the blood-brain barrier may be permeable to particles smaller than ≈ 50 nm.[44,45] In fact, a recent study demonstrated that Cy5-conjugated magnetic NPs, approximately 33 nm in size, were able to cross the blood-brain barrier in mice with brain tumors.[45] However, the NPs were not able to cross the blood-brain barrier in normal mice. Given that our PNPs are approximately 70 to 80 nm in size, they are too large to pass through the blood-brain barrier as a conjugated complex, thus suggesting that the fluorescence observed from the brain was likely from free Cy5 dye.

Another possible concern is the potential of phagocytosis of NPs, especially if they are introduced into tissue with a high concentration of phagocytes (macrophages), such as in or around a tumor-inducing inflammation. Phagocytosis is a principal component of our innate immunity in which macrophages and other antigen-presenting cells internalize large (> 500 nm)
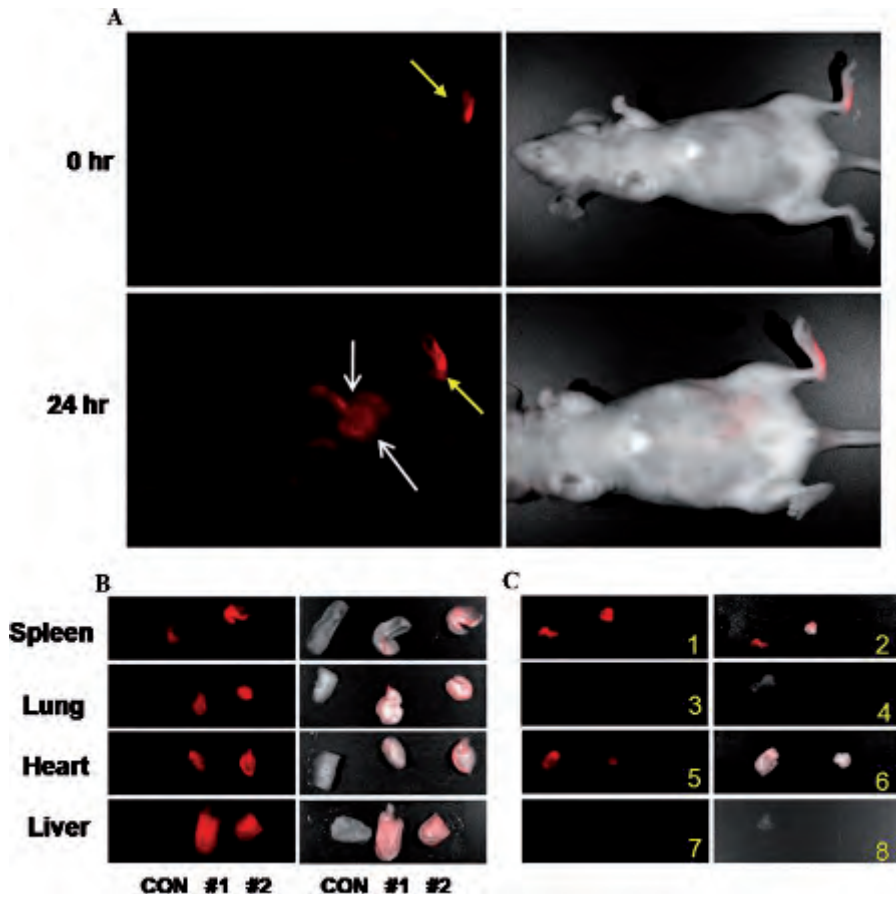
Figure 3. Imaging of Cy5-PNP biodistribution in nude mice. *A*, In vivo fluorescence images taken immediately (0 hours) and 24 hours after PNP injection into the left footpad. The *left column* shows fluorescence from the Cy5-PNP biodistribution and the *right column* shows overlay with brightfield images. *Yellow arrows* show the site of injection; *white arrows* show distributing PNPs. *B*, Representative organs from two PNP-injected nude mice (#1 and #2) and one noninjected control nude mouse (CON). The *left columns* show the fluorescence images and the *right columns* show the overlays with brightfield images. No fluorescence is seen in any of the control organs. *C*, Cy5-PNP biodistribution in the left (C1–C4) and right (C5–C8) popliteal lymph nodes. Images C1, C2, C5, and C6 are from two PNP-injected animals and C3, C4, C7, and C8 are from one noninjected control animal. Fluorescence is seen only in the images from the injected animals, with the strongest signal coming from the left popliteal lymph node (injected side) compared to the right popliteal lymph node (noninjected side).
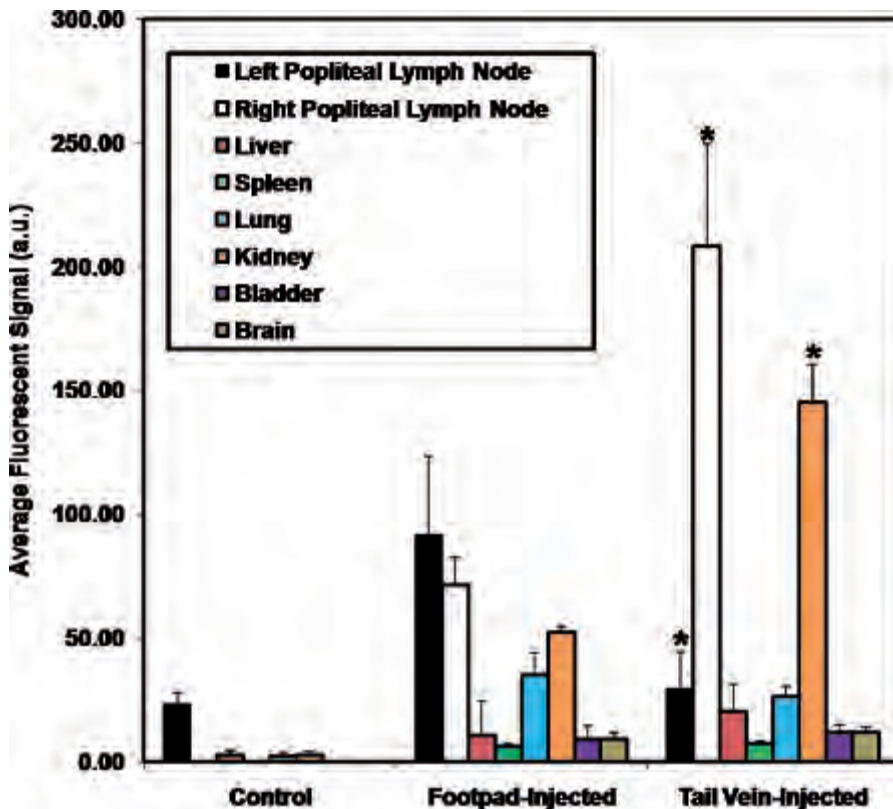
Figure 4. Average fluorescence signal intensities from organs following footpad and tail vein routes of administration. Cy5-PLA PNP were injected into either the lymphatic system via the footpad or the cardiovascular system via the tail vein. *Colored bars* represent the average signal intensity per organ, and *error bars* represent the standard deviation between measured areas of interest within each organ. Statistical analysis confirms lower fluorescence from the left popliteal lymph node and greater fluorescence from the right popliteal lymph node following tail vein injection compared to footpad injection. The statistical analysis also confirms greater fluorescence from the kidney following cardiovascular system delivery compared to delivery via the lymphatic system. *Statistically significant ($p < .05$) compared to the footpad-injected route.
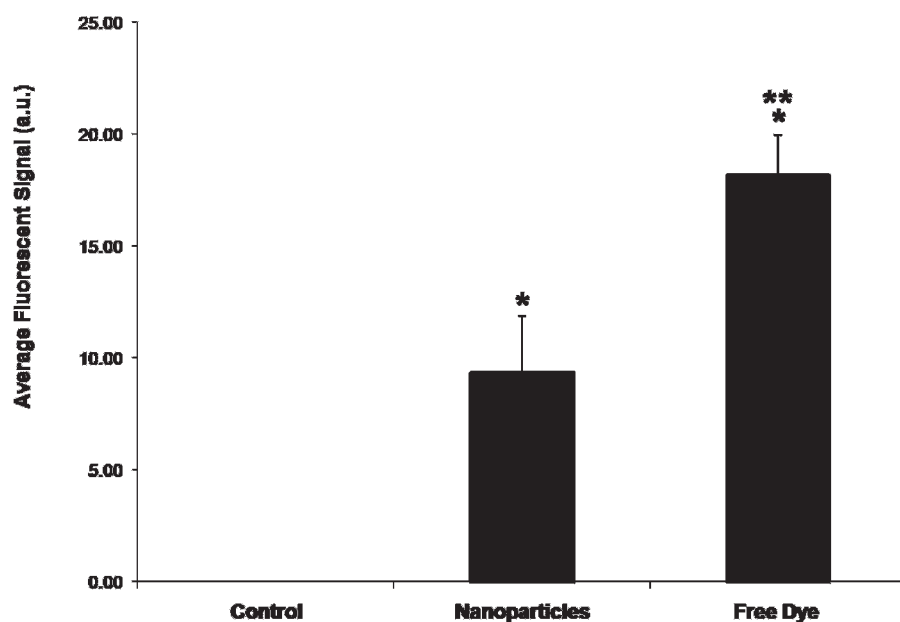
Figure 5. Average fluorescence signal intensity from the brains of footpad-injected animals after 24-hour circulation. One animal was injected with Cy5-PLA PNPs and the other was injected with an equal concentration of free Cy5 dye. Approximately half of the Cy5 dye remains encapsulated inside the PNPs. There was no fluorescence signal detected from the brain of the control animal. *Statistically significant ($p < .05$) compared to the control. **Statistically significant ($p < .05$) compared to the Cy5-PNP complex.

particulate targets.[46] However, given that our NPs are substantially smaller than 500 nm, it is likely that phagocytosis of our NPs will be substantially reduced. In addition to size, the surface property of PNPs can also be critical. It has been reported that for the delivery of subcutaneously administered liposomes to target the lymphatics, liposomes coated with polyethylene glycol (PEG) show reduced macrophage uptake.[47] Given that our NPs are also coated with PEG, we expect them to behave similarly to PEGylated liposomes.

Conclusion

Tumor metastasis is a leading cause of cancer death. It is widely known that cancer will metastasize throughout the body through the lymphatic system, as well as the cardiovascular system. Therefore, to more effectively inhibit or eradicate these metastatic cells, it may be more advantageous to introduce anticancer drugs into both the lymphatic and cardiovascular circulatory systems.

We have demonstrated the feasibility of a potential new strategy for drug delivery that would use the lymphatic circulation to target metastatic disease. Future efforts will investigate the biodistribution dependency on NP size and surface features, as well as the conjugation of cancer treatment drugs, such as docetaxel or paclitaxel, to these PNPs, as has already been done with similar NPs.[17,48,49] The efficacy and toxicity of these drugs conjugated to the PNPs have been evaluated by (3-(4, 5-dimethylthiazol-2-yl)-2, 5-diphenyltetrazolium bromide) (MTT) assay.[19–21] Previously,

we demonstrated that conjugated drugs can be released to their original form, as was determined by NMR studies.[21]

Clinically, these agents may potentially be administered to the interstitial space around primary tumors, just as is currently done with dyes or radiolabels for sentinel lymph node mapping in breast cancer and melanoma surgery.[50,51] Administration of molecularly targeted drug-carrying PNPs into the lymphatic system could be useful not only for detecting and imaging metastatic disease but also for delivering therapeutic drugs to augment therapies that currently only use the cardiovascular circulation for systemic delivery.

Acknowledgment

References

1. Witte MH, Way DL, Witte CL, Bernas M. Lymphagiogenesis: mechanisms, significance and clinical implications. EXS 1997;79: 65–112.

2. Liotta LA, Steeg PS, Stetler-Stevenson WG. Cancer metastasis and angiogenesis: an imbalance of positive and negative regulation. Cell 1991;64:327–36.

3. Weiss L, Schmidschonbein GW. Biomechanical interactions of cancer cells with the microvasculature during metastasis. Cell Biophys 1989;14:187–215.

4. Pepper MS, Tille JC, Nisato R, Skobe M. Lymphangiogenesis and tumor metastasis. Cell Tissue Res 2003;314:167–77.

5. de Boer M, van Deurzen CHM, van Dijck J, et al. Micrometastases or isolated tumor cells and the outcome of breast cancer. N Engl J Med 2009;13:653–63.

6. Elkin MV, Vlodavsky I. Tail vein assay of cancer metastasis. Curr Protoc Cell Biol 2001;19:2.1–2.7.

7. Fidler IJ, Ellis LM. The implications of angiogenesis for the biology and therapy of cancer metastasis. Cell 1994;79:185–8.

8. Hart IR, Fidler IJ. Cancer invasion and metastasis. Q Rev Biol 1980;55:121–42.

9. Liotta LA. Tumor invasion and metastases—role of the extra-cellular matrix: Rhoads Memorial Award lecture. Cancer Res 1986; 46:1–7.

10. Ruoslahti E. How cancer spreads. Sci Am 1996;275:72–7.

11. Kim JH, Kim YS, Park K, et al. Antitumor efficacy of cisplatin-loaded glycol chitosan nanoparticles in tumor-bearing mice. J Control Release 2008;127:41–9.

12. Lee SW, Chang DH, Shim MS, et al. Ionically fixed polymeric nanoparticles as a novel drug carrier. Pharm Res 2007;24:1508–16.

13. Min KH, Park K, Kim YS, et al. Hydrophobically modified glycol chitosan nanoparticles-encapsulated camptothecin enhance the drug stability and tumor targeting in cancer therapy. J Control Release 2008;127:208–18.

14. Ballou B, Ernst LA, Andreko S, et al. Sentinel lymph node imaging using quantum dots in mouse tumor models. Bioconjug Chem 2007;18:389–96.

15. Kim S, Lim YT, Soltesz EG, et al. Near-infrared fluorescent type II quantum dots for sentinel lymph node mapping. Nat Biotechnol 2004;22:93–7.

16. Kobayashi H, Hama Y, Koyama Y, et al. Simultaneous multicolor imaging of five different lymphatic basins using quantum dots. Nano Lett 2007;7:1711–6.

17. Farokhzad OC, Cheng J, Teply BA, et al. Targeted nanoparticle-aptamer bioconjugates for cancer chemotherapy in vivo. Proc Natl Acad Sci U S A 2006;103:6315–20.

18. Cheng J, Teply BA, Sherifi I, et al. Formulation of functionalized PLGA-PEG nanoparticles for in vivo targeted drug delivery. Biomaterials 2007;28:869–76.

19. Tong R, Cheng J. Ring-opening polymerization-mediated controlled formulation of polylactide-drug nanoparticles. J Am Chem Soc 2009;131:4744–54.

20. Tong R, Christian DA, Tang L, et al. Nanopolymeric therapeutics. MRS Bull 2009;34:422–31.

21. Tong R, Cheng J. Paclitaxel-initiated, controlled polymerization of lactide for the formulation of polymeric nanoparticulate delivery vehicles. Angew Chem Int Ed Engl 2008;47:4830–4.

22. Chamberlain BM, Cheng M, Moore DR, et al. Polymerization of lactide with zinc and magnesium beta-diiminate complexes: stereocontrol and mechanism. J Am Chem Soc 2001;123:3229–38.

23. Southwick PL, Ernst LA, Tauriello EW, et al. Cyanine dye labeling reagents—carboxymethylindocyanine succinimidyl esters. Cytometry 1990;11:418–30.

24. Taback B, Hashimoto K, Kuo CT, et al. Molecular lymphatic mapping of the sentinel lymph node. Am J Pathol 2002;161:1153–61.

25. Derfus AM, Chan WCW, Bhatia SN. Probing the cytotoxicity of semiconductor quantum dots. Nano Lett 2004;4:11–8.

26. Kirchner C, Liedl T, Kudera S, et al. Cytotoxicity of colloidal CdSe and CdSe/ZnS nanoparticles. Nano Lett 2005;5:331–8.

27. Guimaraes R, Clement O, Bittoun J, et al. MR lymphography with superparamagnetic iron nanoparticles in rats: pathologic basis for contrast enhancement. AJR Am J Roentgenol 1994;162:201–7.

28. Mouzer R, Shkarin P, Papademetris X, et al. Dynamic imaging of lymphatic vessels and lymph nodes using a bimodal nanoparticulate contrast agent. Lymphat Res Biol 2007;5:151–8.

29. Josephson L, Kircher MF, Mahmood U, et al. Near-infrared fluorescent nanoparticles as combined MR/optical imaging probes. Bioconjug Chem 2002;13:554–60.

30. Galanzha EI, Shashkov EV, Tuchin VV, Zharov VP. In vivo multispectral, multiparameter, photoacoustic lymph flow cytometry with natural cell focusing, label-free detection and multicolor nanoparticle probes. Cytometry A 2008;73:884–94.

31. Galanzha EI, Kokaska MS, Shashkov EV, et al. In vivo fiber-based multicolor photoacoustic detection and photothermal purging of metastasis in sentinel lymph nodes targeted by nanoparticles. J Biophotonics 2009;2:528–39.

32. Allen TM, Cullis PR. Drug delivery systems: entering the mainstream. Science 2004;303:1818–22.

33. Kataoka K, Harada A, Nagasaki Y. Block copolymer micelles for drug delivery: design, characterization and biological significance. Adv Drug Deliv Rev 2001;47:113–31.

34. Ferrari M. Cancer nanotechnology: opportunities and challenges. Nat Rev Cancer 2005;5:161–71.

35. Discher DE, Eisenberg A. Polymer vesicles. Science 2002;297:967–73.

36. Gao XH, Cui YY, Levenson RM, et al. In vivo cancer targeting and imaging with semiconductor quantum dots. Nat Biotechnol 2004; 22:969–76.

37. Lee CC, MacKay JA, Frechet JMJ, Szoka FC. Designing dendrimers for biological applications. Nat Biotechnol 2005;23:1517–26.

38. Musumeci T, Ventura CA, Giannone I, et al. PLA/PLGA nanoparticles for sustained release of docetaxel. Int J Pharm 2006;325:172–9.

39. Mu L, Feng SS. A novel controlled release formulation for the anticancer drug paclitaxel (Taxol(R)): PLGA nanoparticles containing vitamin E TPGS. J Control Release 2003;86:33–48.

40. Avgoustakis K. Pegylated poly(lactide) and ploy(lactide-co-glycolide) nanoparticles: preparation, properties and possible application in drug delivery. Curr Drug Deliv 2004;1:321–33.

41. Galindo-Rodriguez S, Allemann E, Fessi H, Doelker E. Physicochemical parameters associated with nanoparticle formation in the salting-out, emulsification-diffusion, and nanoprecipitation methods. Pharm Res 2004;21:1428–39.

42. Liu J, Meisner D, Kwong E, et al. A novel trans-lymphatic drug delivery system: implantable gelatin sponge impregnated with PLGA-paclitaxel microspheres. Biomaterials 2007;28:3236–44.

43. Weiss L, Ward PM. Lymphogenous and hematogenous metastasis of Lewis lung carcinoma in the mouse. Int J Cancer 1987; 40:570–4.

44. Veiseh O, Sun C, Gunn J, et al. Optical and MRI multifunctional nanoprobe for targeting gliomas. Nano Lett 2005;5:1003–8.

45. Veiseh O, Sun C, Fang C, et al. Specific targeting of brain tumors with an optical/magnetic resonance imaging nanoprobe across the blood-brain barrier. Cancer Res 2009;69:6200–7.

46. Aderem A, Underhill DM. Mechanisms of phagocytosis in macrophages. Annu Rev Immunol 1999;17:593–623.

47. Oussoren C, Storm G. Liposomes to target the lymphatics by subcutaneous administration. Adv Drug Deliver Rev 2001;50:143–56.

48. Farokhzad OC, Cheng J, Teply BA, et al. Targeted nanoparticle-aptamer bioconjugates for cancer chemotherapy in vivo. Proc Natl Acad Sci U S A 2006;103:6315–20.

49. Frangioni JV. In vivo near-infrared fluorescence imaging. Curr Opin Chem Biol 2003;7:626–34.

50. Cody HS. Sentinel lymph node mapping in breast cancer. Breast Cancer 1999;6:13–22.

51. Gipponi M, Bassetti C, Canavese G, et al. Sentinel lymph node as a new marker for therapeutic planning in breast cancer patients. J Surg Oncol 2004;85:102–11.